Low-density Lipoprotein Receptor-related Protein 5 (LRP5)-deficient Rats Have Reduced Bone Mass and Abnormal Development of the Retinal Vasculature

John L. Ubels[1,2], Cassandra R. Diegel[1], Gabrielle E. Foxa[1], Nicole J. Ethen[1], Jonathan N. Lensing[1], Zachary B. Madaj[3], VARI Vivarium and Transgenics Core[3], and *Bart O. Williams[1]

[1] Program for Skeletal Disease and Tumor Microenvironment and Center for Cancer and Cell Biology, Van Andel Research Institute, Grand Rapids, Michigan, United States of America

[2] Department of Biology, Calvin University, Grand Rapids, Michigan, United States of America

[3]Van Andel Research Institute Core Technologies and Services, Grand Rapids, Michigan, United States of America

*Corresponding author

e-mail: bart.williams@vai.org

Abstract

Human patients carrying homozygous loss-of-function mutations in the low-density lipoprotein receptor related protein 5 (*LRP5*) develop osteoporosis pseudoglioma (OPPG), a syndrome characterized by early-onset low bone mass and vision problems caused by abnormal vasculature of the eye. Lrp5-deficient mice have been created and are valuable models for OPPG, however rat models have not been previously developed. Work in several fields suggests that rats have advantages over mice in modeling human physiology. In addition, their larger organs relative to mice, provide increased tissue sample size and easier surgical manipuations, while requiring similar laboratory housing and husbandry. We used CRISPR/Cas9-mediated genetic engineering to create three strains of LRP5-deficient rats. We found that they modelled the low bone mass seen in their human and mouse counterparts. Facilitated by their increased size relatively to mice, we also carried out detailed assessment of ocular vascularization and found that the superficial retinal vasculature is sparse and disorganized with decreases vascularized area, vessel length and branch point density. Extensive exudates suggest increased vessel permeability. These rat models should be useful for further studies of the role of Wnt signaling in bone and retina development and research on treatment of osteoporosis and familial exudative vitroretinopathy.

Introduction

Wnt signaling plays key roles in development, and alterations in the pathway are among the most common events associated with human disease [1, 2]. Wnt ligands initiate cellular responses by binding to a receptor complex that includes a member of the Frizzled family of seven-transmembrane spanning receptors and either low-density lipoprotein receptor-related protein 5 or 6 (LRP5 or LRP6) [1]. Activation of this receptor complex inhibits the phosphorylation of the β-catenin protein by glycogen synthase kinase 3 (GSK3), which normally targets β-catenin for ubiquitin-dependent proteolysis. Thus, β-catenin protein is stabilized in the cytoplasm, and it can subsequently translocate to the nucleus and activate target gene transcription.

Almost 20 years ago, homozygous inactivating mutations in *Lrp5* were causally linked to the human syndrome, osteoporosis pseudoglioma (OPPG) [3, 4]. Patients with OPPG develop osteoporosis in early childhood. Subsequent work, using genetically engineered mouse models, demonstrated that LRP5 most likely acts within the osteoblast lineage to regulate bone mass [5-9]. A large body of additional work further linked alterations in genes whose protein products interact with LRP5, or the highly homologous LRP6, to changes in human bone mass [1]. Primary among these is sclerostin, a protein which is lost by genetic inactivation in human patients with high bone mass [10]. Antibodies that specifically inactivate sclerostin are the basis for the recently FDA-approved drug, romosozumab (EVENITY™, Amgen, Thousand Oaks, CA), which is approved for the treatment of osteoporosis in post-menopausal women at high risk for fracture [11].

OPPG patients often also have severely impaired vision at birth associated with microphthalmia, retinal hypovascularization, and retrolental fibrovascular tissue (pseudoglioma) [12]. A related human hereditary disorder, familial exudative vitreoretinopathy (FEVR) can also be caused by inactivating mutations in *LRP5* [13]. In this case, progressive vision loss is due to abnormal vascularization at the

periphery of the retina [14]. This results in neovascularization in response to oxygen deprivation. The new vessels are leaky due to an impaired blood-retina barrier, resulting in exudates. Impaired vasculature leads to occurrence of retinal detachment and retinal holes. Mutations in other genes linked to the regulation of Wnt signaling, including Frizzled 4 and Norrin, also cause FEVR and the related retinal vascular disorders, Norrie disease, and Coats disease [14, 15].

Consistent with work in the skeletal system, genetically engineered mouse models have also provided insights into the role of LRP5 in development of the retinal vasculature. Whereas normally development of the superficial vasculature is complete by postnatal day 8, and the deeper vasculature is complete by P21, in LRP5 null mice vascular development is delayed, the vessels do not reach the periphery of the retina and the deeper layers of the retinal vasculature do not develop. Neovascularization then occurs due to hypoxia, with development of microaneurysms and vascular tufts [12, 16-18]. Fluorescein angiography reveals an impaired blood-retinal barrier [19].

The laboratory rat at one time was commonly used for physiologic studies, and many genetic strains were developed through selective phenotypic breeding. The development of genetically engineered mouse models using embryonic stem cells led to dominance of mice in biomedical studies, however these mouse models are associated with some limitations. The relatively small size of mice confers a significant advantage in housing and husbandry costs, but while both mice and rats are rodents, functional differences exist, and it has been observed that genetically, mice and rats may be no more closely related than humans and old world monkeys [20, 21]. On the other hand, a large physiologic data base suggests that in several fields, including learning and memory, neurologic function and cardiovascular physiology, the rat is a better model for the study of human physiology and pathophysiology [20, 21]. Rats also have larger organs than mice, providing increased tissue sample size and easier dissection and surgical manipuations, while having similar laboratory housing requirements

and costs. The gene editting technology, CRISPR/Cas9, allowed the re-emergence of the rat as a key model organism in studying human disease, arguing for the expansion of genetically engineered rat models [22]. Development of genetically engineered rodents using embryonic stem cell-based methods can take over 6. In contrast, CRISPR/Cas9 technology allows development of genetically modified rodents in only 2 months with greater predictability, and the ability to modify genes in zygotes makes it more feasible to use rats for such studies. Already genetically modified rats are being used in studies of neurophysiology and cardiovascular disease [23-26].

Mouse models have allowed significant insights into LRP5 function, but for reasons cited above, rats are expected to provide new insights into the function of this Wnt co-receptor. In the present study, we used CRISPR-Cas9-mediated methods to create three strains of rats carrying inactivation mutations in th second exon of the *Lrp5* gene: 1.) An 18 bp deletion, 2.) a 22 bp deletion, and 3.) a strain with an inversion and 11 bp and 3 bp deletions. Studies were conducted to confirm knockout of the *Lrp5* gene and demonstrate lack of expression of functional LRP5 protein. We report that LRP5-deficient rats develop the low bone mass previously seen in LRP5-deficient humans and mice. The validity of the model is also supported by imaging and quantitative analysis of the retinal vasculature, showing that adult $Lrp5^{KO/KO}$ rats with impaired bone development also have a FEVR-like phenotype. At the time of this report, ours is only the second in vivo study of the retina in rats using CRISPR/Cas9 gene editing technology [27]. This rat model for the study of LRP5 function will allow for advantages relative to mice in orthopedic [28] and ophthalmologic [29] research.

Methods

Experimental Animals

Spague-Dawley rats were maintained in accordance with institutional animal care and use guidelines, and experimental protocols were approved by the Institutional Animal Care and Use Committee of the Van Andel Institute.

Generation of *Lrp5* knockout rats using CRISPR/Cas9

Three rat lines with a deletion in *Lrp5* were created using a modified CRISPR/Cas9 protocol [30] Briefly, two sgRNAs targeting exon 2 of *Lrp5* were designed using the MIT guide sequence generator (crispr.mit.edu.) against rn5 genome reference sequence. We used forward guide CCGCCGGGATGTACGACTAGTGG and reverse guide GTTGGCCACCTCGATGCGGTTGG. The guide sequences were then cloned into vector pX330-U6-Chimeric_BB-CBh-hSpCas9 which was a gift from Feng Zhang (Addgene plasmid # 42230; http://n2t.net/addgene:42230 ; RRID:Addgene_42230). The T7 promoter was added to the sgRNA template, and the sequence was synthetized by IDT. The PCR amplified T7-sgRNA product was used as template for *in vitro* transcription using the MEGAshortscript T7 kit (Thermo Fisher Scientific, Waltham, MA). The microinjection mix consisted of Cas9 mRNA (Sigma Aldrich, St. Louis, MO) (final concentration of 40 ng/ul) and sgRNA's (20 ng/ul) in injection buffer (10 mM Tris; 0.1 mM EDTA pH 7.5) injected into the pronucleus of Sprague-Dawley (Charles River Laboratories, Wilmington, MA) zygotes. After identifying founders we backcrossed the line to wildtype Sprague-Dawley rats twice before intercrossing to generate animals for our study.

Genotyping by PCR-HMA and amplicon sequencing

Genomic DNA from rat tail biopsies was isolated by alkaline digestion. To genotype *Lrp5* knockout rats we used the following primers: *Lrp5*-E2-Fwd (CCTCACCACTCCTGTTGTTT) and *Lrp5*-E2-Rev (CCTGCCAGAAGAGAACCTTAC) to amplify a 354bp product. Anticipating that our founders would have small deletions we used a heteroduplex mobility assay [31] to define genotypes. Amplicons were subjected to denaturation-slow renaturation to facilitate formation of heteroduplexes using a

thermocycler. Samples were resolved on polyacrylamide gels (10%) and mobility profiles were used to define genotypes. PCR using the genotyping primers above was performed to amplify indels for each founder for sequencing. The amplified products were cloned using the NEB PCR cloning kit (New England Biolabs, Ipswich, MA). Clones from each founder were Sanger sequenced using the NEB analysis primers to define indels.

Immunoblot analysis

Immunoblots were conducted to confirm lack of expression of functional LRP5 protein. Protein was isolated from rat tail biopsies in lysis buffer (50 mM Na_2HPO_4, 1 mM sodium pyrophosphate, 20 mM NaF, 2 mM EDTA, 2 mM EGTA, 1% Triton X-100, 0.5 mM DTT, protease inhibitor tablet (Roche, Basal, Switzerland) using lysing matrix M (MP Biomedicals, Irvine, CA) for homogenization in the FastPrep-24 sample disruption instrument (MP Biomedicals). The samples were centrifuged at 21,000 x g for 30 minutes at 4 °C to pellet non-lysed tissue. We analyzed 40 μg of protein by SDS-polyacrylamide gel electrophoresis on an 8% Tris-Glycine gel (Thermo Fisher Scientific) and transferred overnight at 4 °C. Immunoblotting was performed using the following antibodies: Lrp5 (D80F2) Rabbit mAb (Cell Signaling, 5731), β-Actin (13E5) Rabbit mAb (Cell Signaling, 5125) (Cell Signalling Technology, Danvers, MA) and V5 Tag mAb,HRP (Thermo Fisher Scientific, R96125).

Plasmid Construction

As will be shown, a gene product was expressed by the rat strain with an 18 bp deletion in the *Lrp5* gene. To assess its potential signaling activity, site-directed mutagenesis was used to generate a human *LRP5* construct with the same 18 bp deletion as the rat model. We previously generated a human *LRP5*-V5 plasmid [32] and we used the Q5 site-directed mutagenesis kit (New England Biolabs) with forward primer (CTCAATGGCACATCCCGG) and reverse primer (GTTGGTCTCTGAGTCCGTC) to generate human *LRP5*-131-136aaΔ-V5. The plasmid was sequenced to confirm the correct modification.

Cell Culture, Transient Transfections, and Reporter Studies

Twelve-well plates coated with poly-d-lysine were seeded with equal amounts of human 293T-Super Top Flash (STF) cells [33]. Cells were transfected by XtremeGene HP as per the manufacturer's specifications (Roche). When cells were about 80% confluent a total of 500 ng of plasmid DNA was transfected per well. To measure the ability of constructs to activate a TCF-dependent reporter, 293T-STF cells were co-transfected with 166 ng of plasmid to be tested, 166 ng of pCDNA3.1-lacZ plasmid, and empty vector DNA was added to normalize the total amount of DNA in each transfection. Transfections were performed in duplicate. Cells were harvested 36 h after transfection by lysing in 100 µl of 1× reporter lysis buffer (Promega, Madison, WI). Lysates were pelleted, and 10 µl of each supernatant was added to 50 µl of luciferase assay substrate (Promega). We used a Synergy Neo HTS multimode microplate reader (BioTek, Winnoski, VT) to measure luciferase activity and readings were normalized for transfection efficiency by measuring β-galactosidase activity as previously described [34]. Luciferase and β-galactosidase activity were measured in duplicate. A linear mixed-effects model with random intercepts to account for repeated sampling via tech reps was used to analyze these data via lmer in R v3.6.0 (https://cran.r-project.org/). Luciferase measures were log2 transformed to improve model fit based on normality of residuals. B-gal was included as a fixed-effect to adjust for varying levels of success for the transfection. Linear contrasts with a Benjamini-Hochberg adjustment for multiple testing were used to test specific two-sided hypotheses of interest while maintaing a 5% false discovery rate. To check protein expression from the various expression constructs, the pellets were resuspended in 1× SDS sample buffer, boiled for 10 min, passed through a 26-gauge needle five times, and analyzed by SDS-PAGE followed by Western blot.

Femoral Bone Mineral Density Analysis by DXA

Rat femoral aerial bone mineral density (BMD) was measured by dual-energy X-ray absorptiometry (DXA) using a PIXImus II bone densitometer (GE Lunar) [5]. Rats were anesthetized via inhalation of 2% isoflurane (Henry Schein, Melville, NY) with oxygen (1.0 L/min) for 10 min prior to imaging and during the procedure (≤ 5 min). The right hindlimb was placed on a specimen tray in the densitometer for analysis. Bone mineral density was calculated by the PIXImus software based on the defined active bone area of the femur.

Micro-Computed Tomography

Femur morphology of rats was evaluated using the SkyScan 1172 micro-computed tomography (μCT) system (Bruker MicroCT, Kontich, Belgium). Femurs from 6 month rats were isolated, fixed in 10% neutral buffered formalin at room temperature for 48 hours, and transferred to 70% ethanol for storage. Femurs were scanned in a 70% ethanol solution using 2000 x 1200 pixel resolution and 7 μm image pixel size. An X-ray voltage of 70 kV, current of 142 μA, and 0.5mm aluminum filter were used. 2D cross-sectional images of the femurs were reconstructed using the reconstruction software, NRecon 1.7.4.6 (Bruker MicroCT). A volume of interest (VOI) was defined using DataViewer 1.5.6.3 (Bruker MicroCT) and a region of interest (ROI) was defined using CTAn 1.18.8.0 (Skyscan, Bruker). The ROI for trabecular bone was drawn in the distal epiphysis, with a defined height of 3.08 mm beginning 0.775 mm proximal from the growth plate. The ROI for cortical bone was 1.002 mm in height and began 7.002 mm from the growth plate. Average thresholds were calculated from trabecular and cortical grayscale images separately and were used to run 2D and 3D analysis for cortical bone and trabecular bone, respectively. Parameters measured for trabecular bone include bone mineral density (BMD), bone volume/tissue volume (BV/TV), trabecular thickness, trabecular separation, and trabecular number, while parameters measured for cortical bone include tissue mineral density (TMD), tissue area, bone area, cortical area fraction (bone area/tissue area), and cross-sectional thickness. Representative images were generated using CTvol 2.3.2.0 (Bruker MicroCT).

RStudio Version 1.1.453 was used to determine statistical significance for DEXA and µCT parameters. For percentage values, p-values were calculated using a beta linear regression model along with a least square means model. For all other values, p-values were calculated by using a generalized linear model along with a least square means model.

Retinal Fixation, Staining and Imaging

Rats were humanely euthanized with CO_2, the eyes were removed, and a 2 mm incision was made at the corneo-scleral limbus. The eyes were fixed in 4% paraformaldehyde in PBS for 1 hour. The corneas and lenses were then removed and fixation continued for 3 hours. Retinas were removed from the eyecups and incubated for 2 hours in 1% Triton X-100 in PBS. Alexa Fluor 594-conjugated *Giffonia simplifolia* isolectin B_4 with an excitation at 594nm and emission at 617nm (Thermo Fisher Scientific) was dissolved in PBS containing 0.5 mM $CaCl_2$. The retinas were incubated overnight at 4°C in isolectin B_4, which binds to the glycocalyx of vascular endothelial cells. The retinas were washed in PBS for 1.5 hours, flat mounted on Superfrost slides (Fisher Scientific) and cover-slipped in Prolong Gold antifade reagent (Fisher Scientific).

Fluorescent images of the retinal vasculature were captured using a Zeiss Axio Imager A2 microscope, ET – DAPI/FITC/Texas Red filter (Carl Zeiss AG, Oberkochen, Germany) and BIOQUANT OSTEO 2019 v19.2.60 software (BIOQUANT Image Analysis Corp., Nashville, TN). The vascular networks were quantified using AngioTool software (http://angiotool.nci.nih.gov;) [35]. This open-source software measures vascular density (% vessels/total area), vessel length and branching index (branch points/mm^2). Data were analyzed by Kruskal-Wallis one-way ANOVA on ranks and Dunn's method using SigmaPlot 12 (Systat Software, Inc., San Jose, CA).

Results

Three independent rat lines carrying deletions in exon 2 of *Lrp5* were created by CRISPR/Cas9-mediated germline modification. Two CRISPR/sgRNAs specific for exon 2 of *Lrp5* were co-injected with Cas9 mRNA into one-cell-stage Sprague-Dawley rat embryos, then subsequently transferred to pseudopregnant females. A total of 15 pups were born with 3 pups containing indels within exon 2. Indels were identified by PCR amplification followed by a heteroduplex mobility assay (HMA). HMA profiles were gel isolated, cloned, and Sanger sequencing revealed a founder with an 18 bp deletion, designated *Lrp5*^{KO1}, and a second founder with a 22 bp deletion at the sgRNA2 site, designated *Lrp5*^{KO2} (Fig. 1A). A third founder, designated Lrp5^{KO3}, had an inversion coupled with small deletions in the exon at both the sgRNA1 (11 bp) and sgRNA2 sites (3 bp) (Fig. 1B). These 3 founder rats were then crossed with wild type rats resulting in germline transmission of each of the three modified alleles. We then intercrossed rats heterozygous for each of these mutations and collected tail tissue for evaluation of protein levels of LRP5 from each of these three alleles. Consistent with the predicted frameshifts associated with *Lrp5*^{KO2} with a 22 bp deletion and *Lrp5*^{KO3} containing the inverted allele, we could not detect LRP5 protein in rats homozygous for these mutations (Fig. 1C). Interestingly, *Lrp5*^{KO1} containing the 18 bp deletion had detectable LRP5 protein (Fig. 1C). This deletion results in loss of amino acids 131 through 136 which encodes the amino acid sequence, RIEVAN, within the first β-propeller (hereafter referred to as *LRP5* $^{\Delta 131\text{-}136}$).

Fig. 1. Description of Lrp5-deficient alleles created by CRISPR/Cas9-mediated genomic editing in the rat. Two sgRNAS (sgRNA1 and sgRNA2 with the PAM sequence noted) were injected with Cas9 into rat embryos to induce alterations within Exon 2 of *Lr*p5. **A.** Two alelles with deletions were created and characterized, *Lrp5*^{KO1} had an 18 bp deletion (*LRP5* $^{\Delta 131\text{-}136}$) while *Lrp5*^{KO2} carried a 22 bp deletion (indicated by dashes for each bp missing relative to the wild type (WT) sequence shown above)**. B.** A

third modified allele, *Lrp5*^{KO3}, contained a modification caused by an inversion that likely occurred after Cas9-mediated cleavage at both sgRNA sites. In addition to this inversion, two small deletions associated with both sgRNA sites were induced. **C.** Western blot analysis reveals a loss of Lrp5 protein from tissue lysates of rats homozygous for the *Lrp5*^{KO2} and *Lrp5*^{KO3} alleles. Rats homozygous for the *Lrp5*^{KO1} allele express protein (*LRP5* $^{\Delta 131\text{-}136}$) from the modified allele.

To assess whether the in-frame deletion protein expressed in rats homozygous for the *Lrp5*^{KO1} mutation was active in Wnt/β-catenin signaling, we created a cDNA expressing human *LRP5* $^{\Delta 131\text{-}136}$ and measured its ability to activate a stably integrated β-catenin responsive reporter gene (TOPflash) in HEK293T cells [33]. We found that while transfecting a wild-type version of human *LRP5* could activate the β-catenin-responsive TOPflash reporter in conjunction with an Wnt8-Fzd5 fusion proteins [32], *LRP5* $^{\Delta 131\text{-}136}$ could not do so (Fig. 2). This is consistent with the interpretation that the *LRP5* $^{\Delta 131\text{-}136}$ protein expressed in *Lrp5*^{KO1} rats is not capable of supporting Wnt signaling.

Fig. 2. Functional characterization of the *Lrp5*^{KO1} allele-associated protein. **A.** A schematic diagram of the Lrp5 protein shows the region (red) in the first β-propeller motif that contains the 18 bp (6 amino acid in-frame deletion). We hypothesize this blocks the interaction with Wnt ligands. **B**. Transfection of a plasmid expressing the wild type Lrp5 protein, but not that expressed by the ***Lrp5*^{KO1}** allele (Lrp5$^{\Delta 131\text{-}136}$), can the β-catenin-responsive TOPflash reporter in HEK293 cells. A plasmid directing expression of a Wnt8-Fzd5 fusion protein we have previously used to study activation of the TOPflash reporter [30] is co-transfeceted with the two Lrp5 expression plasmids. **C.** The presence of a V5 epitope tag on the C terminus of both the wild type and Lrp5$^{\Delta 131\text{-}136}$ expression plasmids was used to confirm expression of both proteins.

Effect of *Lrp5* Knockout on Bone

To examine the skeletal phenotypes of *Lrp5*$^{KO/KO}$ rats, we analyzed femurs from *Lrp5*^{KO1}, *Lrp5*^{KO2}, and *Lrp5*^{KO3} lines using µCT (Fig. 3). Both sexes in all three lines displayed the same trends in trabecular bone, but varying severities (Fig. 3A). In female and male *Lrp5*$^{KO/KO}$ rats , BMD significantly decreased by 29-81% and BV/TV significantly decreased by 84-192% compared to their controls (Fig. 3B-D). The decrease in bone mass was coupled with a change in trabecular morphology. The overall number of trabeculae in the distal femur of *Lrp5*^{KO1}, *Lrp*^{KO2}, and *Lrp5*^{KO3} rats decreased by 31-96%, 33-40% and 44-48%, respectively (Fig. 3B-D). However, the decrease was only stastistically significant in *Lrp5*^{KO1} and *Lrp5*^{KO3} rats (Fig. 3B and 2D). In addition, the thickness of the trabeculae significantly decreased by 23-93% in all *Lrp5*$^{KO/KO}$ rats, resulting in greater separation between trabeculae (Fig. 3B-D). This increase in trabecular separation was significant in all *Lrp5*$^{KO/KO}$ rats with the exception of *Lrp5*^{KO2} female rats (Fig. 3C). Ultimately, the Lrp5 deficiency in *Lrp*^{KO1}, *Lrp5*^{KO2}, and *Lrp*^{KO3} rats negatively impacted trabecular bone framework.

Fig 3. *Lrp5*-deficient rats display decreased trabecular bone mass and quality. (A) Representative µCT images of the trabecular bone region analyzed from the distal femur of *Lrp5*^{KO1}, *Lrp5*^{KO2}, and *Lrp5*^{KO3} rats. (B) Quantitative analysis of *Lrp5*^{KO1} rats, bone mineral density (BMD), bone volume/tissue volume (BV/TV), trabecular thickness, trabecular separation, and trabecular number, n=4-6. (C) Quantitative analysis of *Lrp5*^{KO2} rats, bone mineral density (BMD), bone volume/tissue volume (BV/TV), trabecular thickness, trabecular separation, and trabecular number, n=5. (D) Quantitative analysis of *Lrp5*^{KO3} rats, bone mineral density (BMD), bone volume/tissue volume (BV/TV), trabecular thickness, trabecular separation, and trabecular number, n = 4-6 (*$p < 0.05$).

Cortical bone architecture was also modified in both sexes (Fig. 4A). While there was no significant change in tissue mineral density (TMD) or cortical area fraction (CAF), the size of femoral

midshaft significantly decreased in *Lrp5*^{KO1}, *Lrp5*^{KO2}, and *Lrp5*^{KO3} rats compared to their controls (Fig. 4B-D). The decrease in cortical bone size is supported by the significant decrease of tissue area and bone area in all *Lrp5*$^{KO/KO}$ rats. The tissue area decrease in mutants ranged from 14-42% in females and 18-34% in males, while bone area decrease ranged from 15-36% in females and 19-31% in males (Fig. 4B-D). Additionally, cortical bone in *Lrp5*^{KO1}, *Lrp5*^{KO2}, and *Lrp5*^{KO3} rats was thinner compared to wild type rats. Cross-sectional thickness significantly decreased by 6-14% in all *Lrp5*$^{KO/KO}$ rats with the exception of *Lrp*^{KO1} females (Fig. 4B-D). Overall, the LRP5-deficency in mutant rats did not did not result in a marked change in cortical bone density, but did culminate in a significant change in cortical structure.

Fig 4. *Lrp5*-deficient rats exhibit a decrease in femoral cortical bone size. (A) Representative µCT images of the cortical bone region analyzed from the femur of *Lrp5*^{KO1}, *Lrp5*^{KO2}, and *Lrp5*^{KO3} rats. (B) Quantitative analysis of *Lrp5*^{KO1} rats, tissue mineral density (TMD), cortical area fraction (CAF, bone area/tissue area), tissue area, bone area, and average cross-sectional thickness, *n*=4-6. (C) Quantitative analysis of *Lrp5*^{KO2} rats, tissue mineral density (TMD), cortical area fraction (CAF, bone area/tissue area), tissue area, bone area, and average cross-sectional thickness, *n*=5. (D) Quantitative analysis of *Lrp5*^{KO3} rats, tissue mineral density (TMD), cortical area fraction (CAF, bone area/tissue area), tissue area, bone area, and average cross-sectional thickness, *n* = 4-6 (*p < 0.05).

Effect of *Lrp5* Knockout on Retinal Vasculature

The retinal vasculature consists of three vascular beds, including a superficial plexus in the nerve fiber layer of the retina, an inner network located in the inner plexiform layer and an outer network in the outer plexiform layer. These parallel beds originate at the optic disc from branches of the central retinal artery and return via the central retinal vein. Ten to twelve large superficial arteries and veins radiate from the optic disc of the rat retina, dividing into the superficial network, as seen in the wildtype

(WT) and heterozygous (KO/+) images in Figures 5 and 6. In contrast to bone, there was no difference in the retinas of male and female rats. Therefore data from the sexes are combined.

Three-month old rats have a completely developed retina vasculature extending to the periphery, with the extensive, well-organized branching pattern expected in wild type animals. The retinas of heterozygous rats show a similar pattern and appear to be normally developed in animals with either the KO1 or KO3 alelle deletion in one *Lrp5* alelle (Figs 5 and 6).

Fig. 5. Effect of an 18 bp deletion in the *Lrp5* gene (*Lrp5*^{KO1}) on vascularization of the retina of 3 month old rats. Flat-mounted retinas of wild type (WT) and heterozygous animals (KO/+) animals stained with isolectin B4 have well-organized blood vessels originating at the optic disc and branching regularly to the retinal periphery. Vessels in retinas from 2 *Lrp5*$^{KO/KO}$rats are sparse and disorganized with reduced branching. Extensive autofluorescent exudates are present. The images are representative of 8 WT, 5 KO/+ and 6 KO/KO rats.

Fig. 6. Effect of inactivation of Lrp5 (*Lrp5*^{KO3}) on vascularization of the retina of 3 month old rats. While the vasculature of WT and KO/+ rats is normal, retinal vessels of *Lrp5*$^{KO/KO}$ rats are sparse and disorganized with reduced branching and vessels ending in vascular tufts (right image). Extensive autofluorescent exudates are present. The images are representative of 6 WT, 7 KO/+ and 8 KO/KO rats.

The superficial retinal vasculature of *Lrp5*$^{KO/KO}$ (both *Lrp5*^{KO1} and *Lrp5*^{KO3} were evaluated) has a severely abnormal phenotype. The number of large vessels radiating from the optic disc is reduced. The vasculature is disorganized, the network of branching, small vessels is nearly absent in large regions of the retina, and in some regions the vessels do not reach the peripheral retina (Figs. 5 and 6). Vessels also may end in blind, “glomerular” tufts (Fig. 6, right KO/KO image). Retinas of rats with a homozygous 22

bp deletion in the *Lrp5* gene (*Lrp5*^{KO2}) also have a sparse retinal vasculature and large regions of exudates (Fig. 7).

Fig. 7. Retinas of 3 month old, homozygous rats with a 22 bp deletion in the *Lrp5* gene (*Lrp*^{KO2}). Exudates and abnormal development of the vasculature are evident. Images are representative of 7 rats.

Quantitative Analysis of the Retinal Vasculature Using AngioTool

To verify that loss function mutations of the *Lrp5* gene cause a retinal vascular phenotype with impaired vascularization, the AngioTool image analysis program was used to quantify the vascularized area, vessel length, and branch point density in retinas of *Lrp5*^{KO1} *and Lrp5*^{KO3} rats. Because of the large regions of exudate in the retinas of *Lrp5*^{KO2} rats (Fig. 7), it was not possible to quantify the vascular pathology in this strain .

It must be noted that in this study vascularized area is defined as the percent of retinal area that is vascularized within a 4 mm^2 digital explant, rather than vascularized area of the entire retina, as reported in previous studies of young mice with an *Lrp5* mutation [16, 18]. Because the large exudates in the *Lrp*$^{KO/KO}$ retinas obscure the vasculature, it was not possible to make measurements of the entire retina of these animals. For this reason, 2 mm X 2 mm (4 mm^2) digital "explants" were analyzed (Fig. 8). These explants were taken from areas of wild type, heterozygous and homozygous animals where the vasculature was fully visible and where there were minimal cuts in the retina that were made in the process of flat mounting. Where possible, two explants were analyzed from the right and left retinas of each animal, although in some retinas it was possible to analyze only 1 explant.

Fig. 8. Representative images of 4 mm^2 digital explants of vascular networks analyzed by AngioTool.

Explants of WT and KO/KO (*Lrp5*^{KO1}) retinas are shown in the left panels. The right panels show Angiotool images with vessels outlined in yellow and highlighted in red while branch points are marked in blue. The program calculates the vascularized area, vessel length, and branch point density.

In rats with a homozygous 18 bp *Lrp5* deletion (*Lrp*^{KO1}) 25.4% of the retina was vascularized. This was significantly different than the 37.7% vascularization of wild type retinas (Fig. 8). The median vessel length of wild type retinas was 1.75 mm, compared to a significant reduction to 0.63 mm in *Lrp5*^{KO1} retinas (Fig. 8). The decreased branching of vessels was especially notable on images of homozygous knock out retinas (Figs. 4, 5 and 6), and analysis showed that in rats with an 18 bp deletion the number of branch points/mm^2 was 86.3/mm^2 in wild type retinas and 42.3/mm^2 in *Lrp5*^{KO1} retinas, a significant reduction (Fig. 9). None of the measured parameters in heterozygous retinas was different from wild type.

Fig. 9. Effect of an 18 bp deletion in the Lrp5 gene (*Lrp5*^{KO1}**) on retinal vasculature.** The vascularized area, vessel length, and number of branch points are significantly reduced in *Lrp5*$^{KO/KO}$ rats*, while the retinas of heterozygous rats (KO/+) are not affected as compared to wild type (WT) rats. (Kruskal-Wallis one-way analysis of variance on ranks and Dunn's method, * $p < 0.05$; number of explants - WT: $n = 37$, KO/+: $n = 23$, KO/KO: $n = 31$)

Inactivation of *Lrp5* by the allelic inversion (*Lrp*^{KO3}) had a similar effect on the retinal vasculature to an 18 bp deletion. Vascularized area was reduced from 40.7% in WT rats to 32.7% in *Lrp5*^{KO3} rats. Median vessel length was reduced from 1.9 mm to 0.9 mm, and median branch point density in the *Lrp5*^{KO3} retinas was only 48.8/mm^2 compared to 97.5/mm^2 in wild type retinas (Fig. 10). All of these

differences were statistically significant. As in rats with an 18 bp deletion, the heterozygous genotype had no effect on the retinal vasculature.

Fig. 10. Loss of Lrp5 (*Lrp5*^{KO3}) reduces the vascularized area, vessel length and number of branch points in rat retinas. Heterozygous (KO/+) retinas have normal vasculature as compared to the wild type (WT). (* $p < 0.05$; number of explants - WT: $n = 29$, KO/+: $n = 37$, KO/KO: $n = 15$).

Discussion

In this study we have successfully produced three strains of rats with loss of function mutations of the *Lrp5* gene. The loss of this co-receptor inhibits Wnt signaling required for normal development of both trabecular and cortical bone. In trabecular bone this results in decreased bone mineral density, bone mass, trabecular thickness and trabecular separation. Cortical bone density did not change, however, bone size was decreased. The *Lrp5* mutations also cause retinal pathology that closely resembles familial exudative vitreoretinopathy. Retinal vascularization is abnormal with reduced area of vascularization and reduced branching of vessels. Notably, the animals have extensive retinal exudates.

We have successfully developed the first rat model of osteoporosis as a result of mutation of the *Lrp5* gene. The availability of this genetically modified rat increases the options available for evaluating osteoporotic therapies and the larger size of the rat relative to the mouse may facilitate assessment of orthopedic procedures in the context of Lrp5 deficiency.

The retinal pathology caused by *Lrp5* knockout was similar in all three rat strains, with no difference between males and females, but some differences were noted compared to previously reported mouse models. The retinas used in this study were from 3-month old, adult rats and have advanced vascular disease. Most previous studies of *Lrp5* knockout mice concentrated on early postnatal development of the retinal vasculature [12, 16-18]. In two studies that included 1-month old mice, a reduced vasculature with vessels ending in tufts is also observed [12, 18], but the vasculature does not appear to be as severely affected as in the rat.

The $Lrp5^{KO/KO}$ rat retinas have extensive, autofluorescent exudates (Figs. 5-7), similar to those seen in human FEVR retinas [14, 17, 36, 37]. These exudates show that the retinal vasculature is leaky with a defective blood-retina barrier. To our knowledge, autofluorescent exudates have not been reported in adult *Lrp5* knockout mouse models, and exudates are not detectable in published images from younger (P7 – P17) *Lrp5* knockout mice [12, 16, 18]. Leakage from retinal vessels of *Lrp5* knockout

mice as been demonstrated experimentally using fluorescein and FITC dextran, and retinal hemorrages were occasionally seen on in vivo fundoscopic images of 2.5-month old *Lrp5* null mice [19]. Taken together, and in agreement with the exudative pathology seen in humans with mutations in the Wnt signaling pathway, our data and the mouse models show that LRP5 is essential to maintenance of the blood-retinal barrier. Chen et al. have reported down regulation of the gene for the tight junction protein, claudin 5, in retinas of *Lrp5* null mice [18], and Diaz-Coranguez et al. have reviewed the literature showing that Wnt signaling and Norrin are essential to the development of the blood-retina barrier [38]. This provides a reasonable explanation for the exudative retinal pathology in *Lrp5* knockout rats.

The anatomy of the retinal vasculature in *Lrp5* knock out rats is comparable to that of *Lrp5* knockout mice although some differences are apparent. The reduction in branch-point density of about 50% in $Lrp5^{KO/KO}$ rats in this study is similar to that reported in P7 mice [16]. A marked reduction in vascular branching was also reported in one month old *Lrp5* null mice [12]. The data show that loss of function of LRP5 in our rat model causes similar changes to those reported in mice, validating this model for studies of the role of Wnt signaling in control of retinal vascular development. In contrast to previously reported studies of mice, our data demonstrate more advanced retinal disease in adult animals. The rats also express the sparce, tortuous retinal vasculature that has been reported in humans with FEVR [36, 37]. Of particular interest are the vessels that end in bulbous tufts in vascular peripheryof $Lrp5^{KO3}$ rats (Fig. 6). Similar bulbous vascular endings have been reported in peripheral retinal vessels of humans with FEVR [36].

The images and quantitative data in this study suggest that the rat retinal pathology may prove to be a very good model of human FEVR. The large regions of exudate in the rats especially appear to be similar to human exudates. Further studies of the rats in vivo, including fundus photography and optical

coherence tomography, similar to data from human with FEVR [37], will be important for testing this hypothesis.

Conclusion

This study supports the feasibility of using CRISPR/Cas9 to produce genetically modified strains of rats. It also reports another model of Osteoporosis pseudoglioma syndrome that may be more amenable to a wider variety of experimental evaluations. Our model of *Lrp5* mutation will be useful in further studies of Wnt signaling in general. More specifically, the presence of bone and retinal pathology in these animals will make these genetic strains useful for research on treatment of osteoporosis and FEVR.

Acknowledgements

This work was funded by the Van Andel Institute and the Calvin Fund for Eye Research. Key members of the VARI Vivarium and Transgenics Core include Bryn Eagleson, Adam Rapp, Nicholas Getz, Audra Guikema, Tristan Kempston, Malista Powers, and Tina Meringa. We thank other members of the Williams Laboratory for their advice and assistance. We thank Karsten Melcher for assistance in preparing Figure 2.

BOW is a member of the Surrozen Scientific Advisory Board Member and a Surrozen stockholder. Work in the Williams Laboratory is partially supported by a sponsored research agreement from Janssen Pharmaceutica. Within the last five years, BOW has been a consultant for Vertex and Amgen.

References

1. Joiner, D.M., et al., *LRP5 and LRP6 in development and disease.* Trends Endocrinol Metab, 2013. **24**(1): p. 31-9.
2. Nusse, R. and H. Clevers, *Wnt/beta-Catenin Signaling, Disease, and Emerging Therapeutic Modalities.* Cell, 2017. **169**(6): p. 985-999.
3. Gong, Y., et al., *LDL receptor-related protein 5 (LRP5) affects bone accrual and eye development.* Cell, 2001. **107**(4): p. 513-23.
4. Maltese, P., et al., *Osteoporosis-pseudoglioma syndrome: Report of two cases and a manifesting carrier.* Ophthalmic Genet, 2017. **38**(5): p. 473-479.
5. Holmen, S.L., et al., *Decreased BMD and limb deformities in mice carrying mutations in both Lrp5 and Lrp6.* J Bone Miner Res, 2004. **19**(12): p. 2033-40.
6. Cui, Y., et al., *Lrp5 functions in bone to regulate bone mass.* Nat Med, 2011. **17**(6): p. 684-91.
7. Joeng, K.S., et al., *Lrp5 and Lrp6 redundantly control skeletal development in the mouse embryo.* Dev Biol, 2011. **359**(2): p. 222-9.
8. Maupin, K.A., C.J. Droscha, and B.O. Williams, *A Comprehensive Overview of Skeletal Phenotypes Associated with Alterations in Wnt/beta-catenin Signaling in Humans and Mice.* Bone Res, 2013. **1**(1): p. 27-71.
9. Riddle, R.C., et al., *Lrp5 and Lrp6 exert overlapping functions in osteoblasts during postnatal bone acquisition.* PLoS One, 2013. **8**(5): p. e63323.
10. Williams, B.O., *Insights into the mechanisms of sclerostin action in regulating bone mass accrual.* J Bone Miner Res, 2014. **29**(1): p. 24-8.
11. *Romosozumab (Evenity) for postmenopausal osteoporosis.* Med Lett Drugs Ther, 2019. **61**(1573): p. 83-86.
12. Huang, W., et al., *Critical Endothelial Regulation by LRP5 during Retinal Vascular Development.* PLoS One, 2016. **11**(3): p. e0152833.
13. Toomes, C., et al., *Mutations in LRP5 or FZD4 underlie the common familial exudative vitreoretinopathy locus on chromosome 11q.* Am J Hum Genet, 2004. **74**(4): p. 721-30.
14. Gilmour, D.F., *Familial exudative vitreoretinopathy and related retinopathies.* Eye (Lond), 2015. **29**(1): p. 1-14.
15. Warden, S.M., C.M. Andreoli, and S. Mukai, *The Wnt signaling pathway in familial exudative vitreoretinopathy and Norrie disease.* Semin Ophthalmol, 2007. **22**(4): p. 211-7.
16. Wang, Z., et al., *Pharmacologic Activation of Wnt Signaling by Lithium Normalizes Retinal Vasculature in a Murine Model of Familial Exudative Vitreoretinopathy.* Am J Pathol, 2016. **186**(10): p. 2588-600.
17. Wang, Z., et al., *Wnt Signaling in vascular eye diseases.* Prog Retin Eye Res, 2019. **70**: p. 110-133.
18. Chen, J., et al., *Retinal expression of Wnt-pathway mediated genes in low-density lipoprotein receptor-related protein 5 (Lrp5) knockout mice.* PLoS One, 2012. **7**(1): p. e30203.
19. Xia, C.H., et al., *A model for familial exudative vitreoretinopathy caused by LPR5 mutations.* Hum Mol Genet, 2008. **17**(11): p. 1605-12.
20. Homberg, J.R., M. Wohr, and N. Alenina, *Comeback of the Rat in Biomedical Research.* ACS Chem Neurosci, 2017. **8**(5): p. 900-903.
21. Neff, E.P., *CRISPR improves prospects for transgenic rats.* Lab Animal, 2019. **48**(6): p. 167-167.
22. *Rats!* Nat Methods, 2010. **7**(6): p. 413.
23. Back, S., et al., *Neuron-Specific Genome Modification in the Adult Rat Brain Using CRISPR-Cas9 Transgenic Rats.* Neuron, 2019. **102**(1): p. 105-119 e8.
24. Ma, Y., et al., *Heritable multiplex genetic engineering in rats using CRISPR/Cas9.* PLoS One, 2014. **9**(3): p. e89413.

25. Cheng, X., et al., *Positional cloning of quantitative trait nucleotides for blood pressure and cardiac QT-interval by targeted CRISPR/Cas9 editing of a novel long non-coding RNA.* PLoS Genet, 2017. **13**(8): p. e1006961.
26. Waghulde, H., et al., *Attenuation of Microbiotal Dysbiosis and Hypertension in a CRISPR/Cas9 Gene Ablation Rat Model of GPER1.* Hypertension, 2018. **72**(5): p. 1125-1132.
27. Bakondi, B., et al., *In Vivo CRISPR/Cas9 Gene Editing Corrects Retinal Dystrophy in the S334ter-3 Rat Model of Autosomal Dominant Retinitis Pigmentosa.* Mol Ther, 2016. **24**(3): p. 556-63.
28. Schindeler, A., et al., *Preclinical models for orthopedic research and bone tissue engineering.* J Orthop Res, 2018. **36**(3): p. 832-840.
29. Flannery, J.G., *Transgenic Animal Models for the Study of Inherited Retinal Dystrophies.* ILAR J, 1999. **40**(2): p. 51-58.
30. Cong, L. and F. Zhang, *Genome engineering using CRISPR-Cas9 system.* Methods Mol Biol, 2015. **1239**: p. 197-217.
31. Challa, A.K., et al., *Novel Hypomorphic Alleles of the Mouse Tyrosinase Gene Induced by CRISPR-Cas9 Nucleases Cause Non-Albino Pigmentation Phenotypes.* PLoS One, 2016. **11**(5): p. e0155812.
32. Holmen, S.L., et al., *A novel set of Wnt-Frizzled fusion proteins identifies receptor components that activate beta -catenin-dependent signaling.* J Biol Chem, 2002. **277**(38): p. 34727-35.
33. Xu, Q., et al., *Vascular development in the retina and inner ear: control by Norrin and Frizzled-4, a high-affinity ligand-receptor pair.* Cell, 2004. **116**(6): p. 883-95.
34. Williams, B.O., et al., *A comparative evaluation of beta-catenin and plakoglobin signaling activity.* Oncogene, 2000. **19**(50): p. 5720-8.
35. Zudaire, E., et al., *A computational tool for quantitative analysis of vascular networks.* PLoS One, 2011. **6**(11): p. e27385.
36. Kashani, A.H., et al., *Diversity of retinal vascular anomalies in patients with familial exudative vitreoretinopathy.* Ophthalmology, 2014. **121**(11): p. 2220-7.
37. Yonekawa, Y., et al., *Familial Exudative Vitreoretinopathy: Spectral-Domain Optical Coherence Tomography of the Vitreoretinal Interface, Retina, and Choroid.* Ophthalmology, 2015. **122**(11): p. 2270-7.
38. Diaz-Coranguez, M., C. Ramos, and D.A. Antonetti, *The inner blood-retinal barrier: Cellular basis and development.* Vision Res, 2017. **139**: p. 123-137.

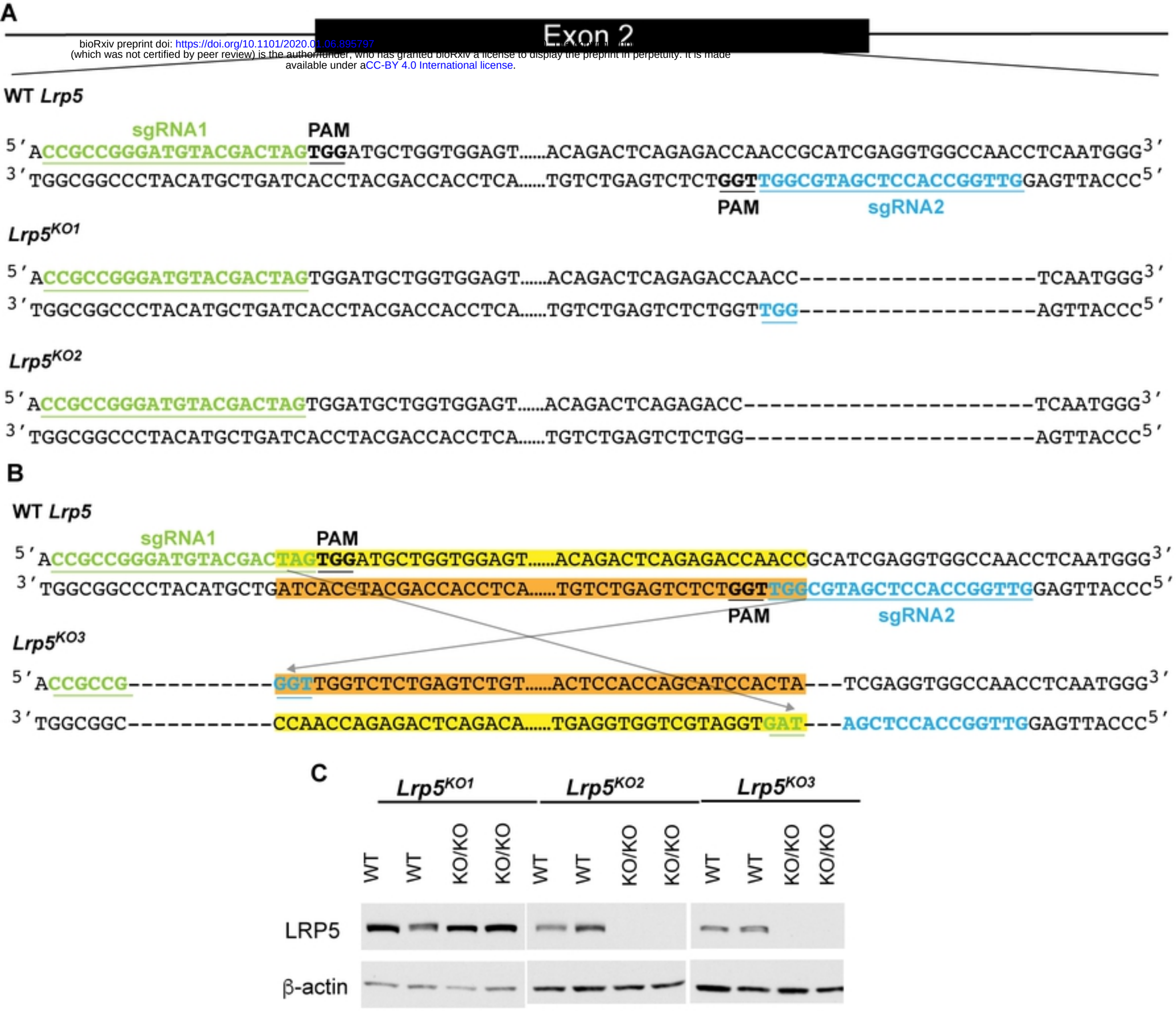

Figure 1

A

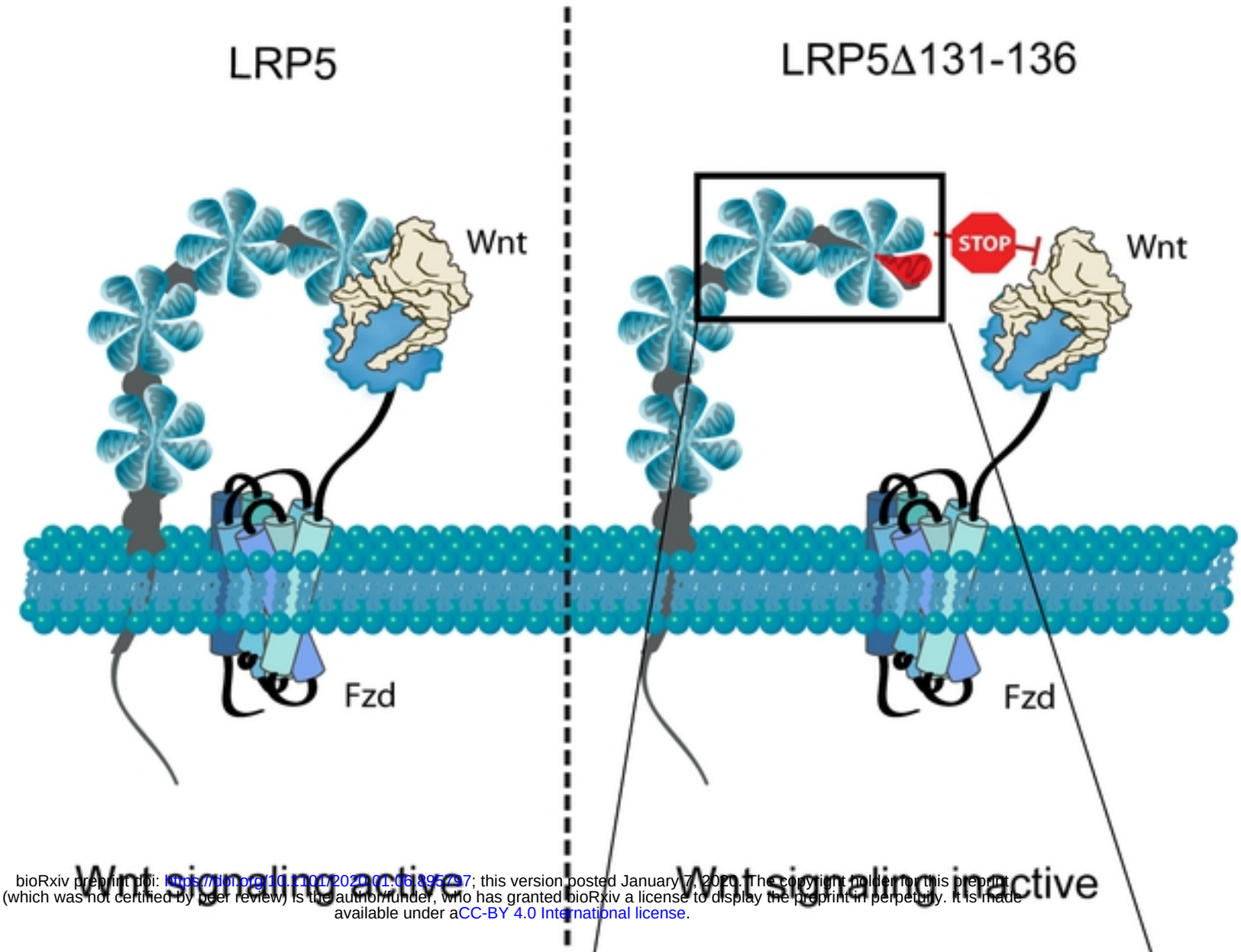

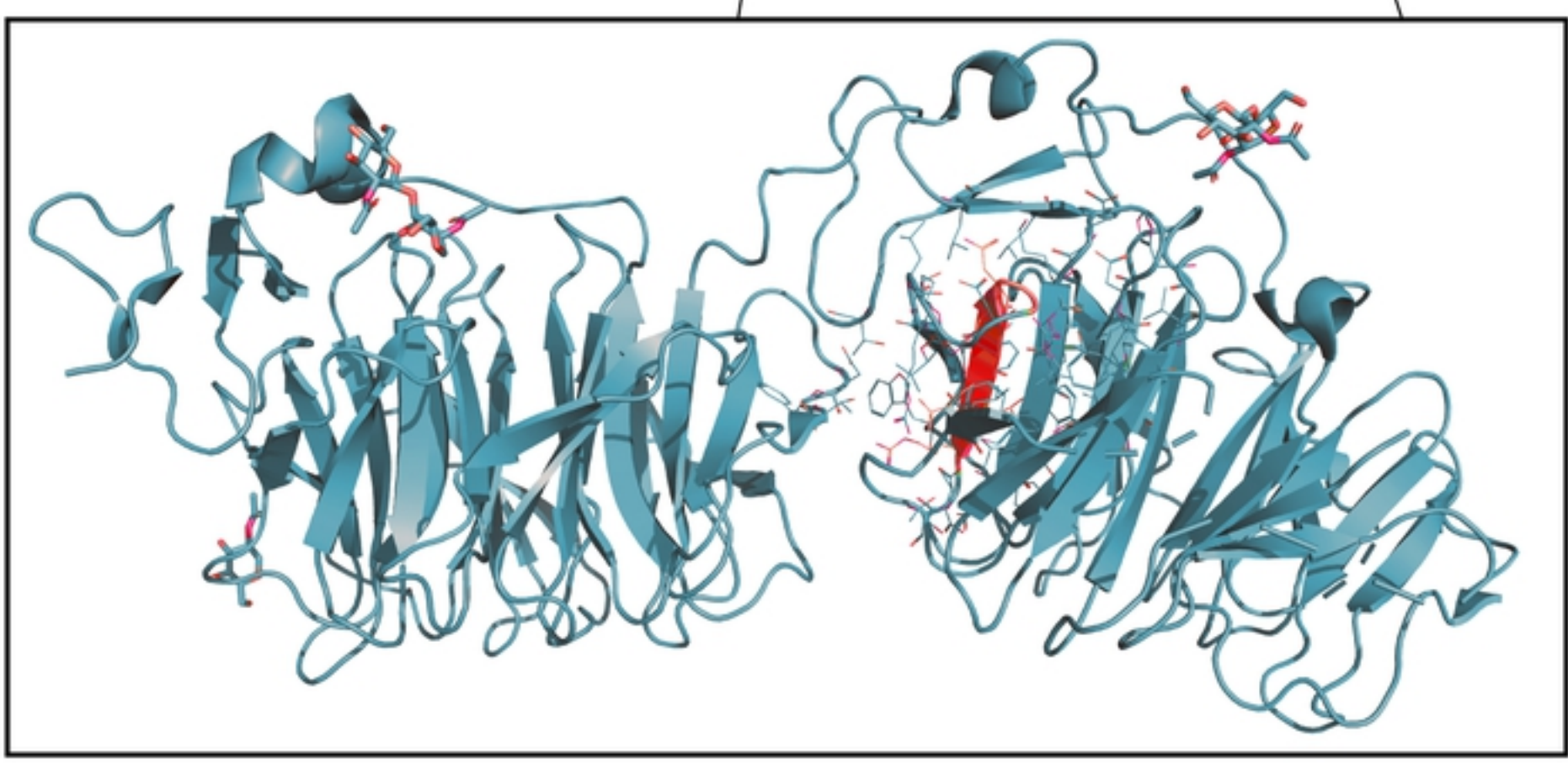

B

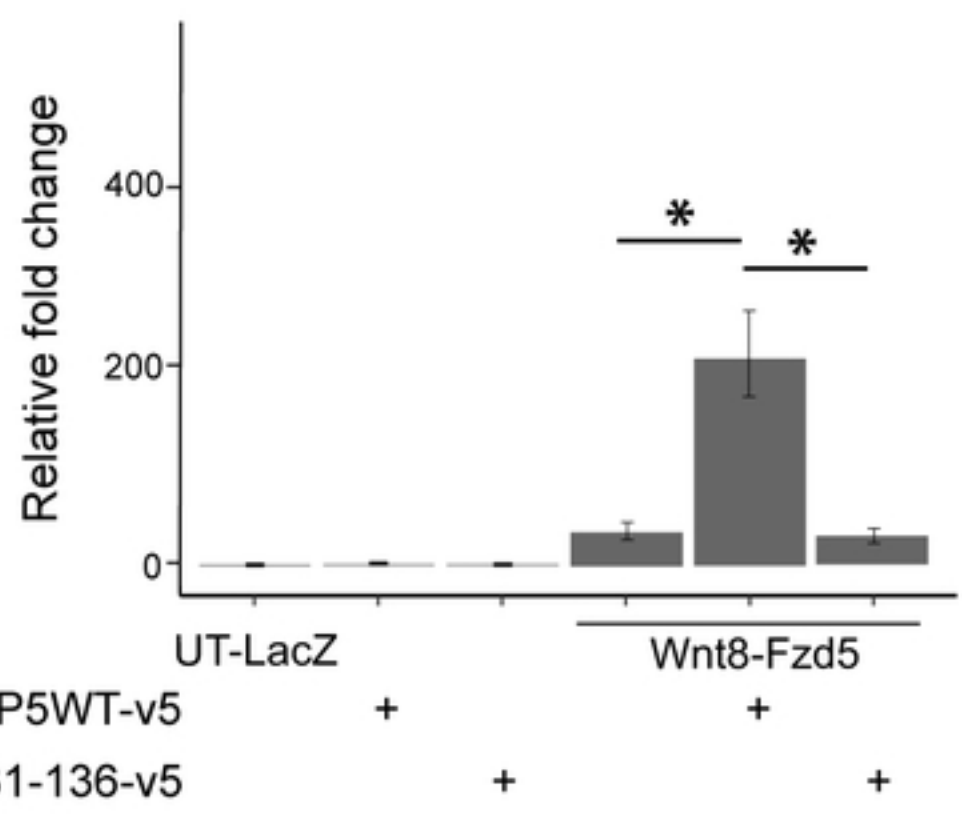

C

Figure 2

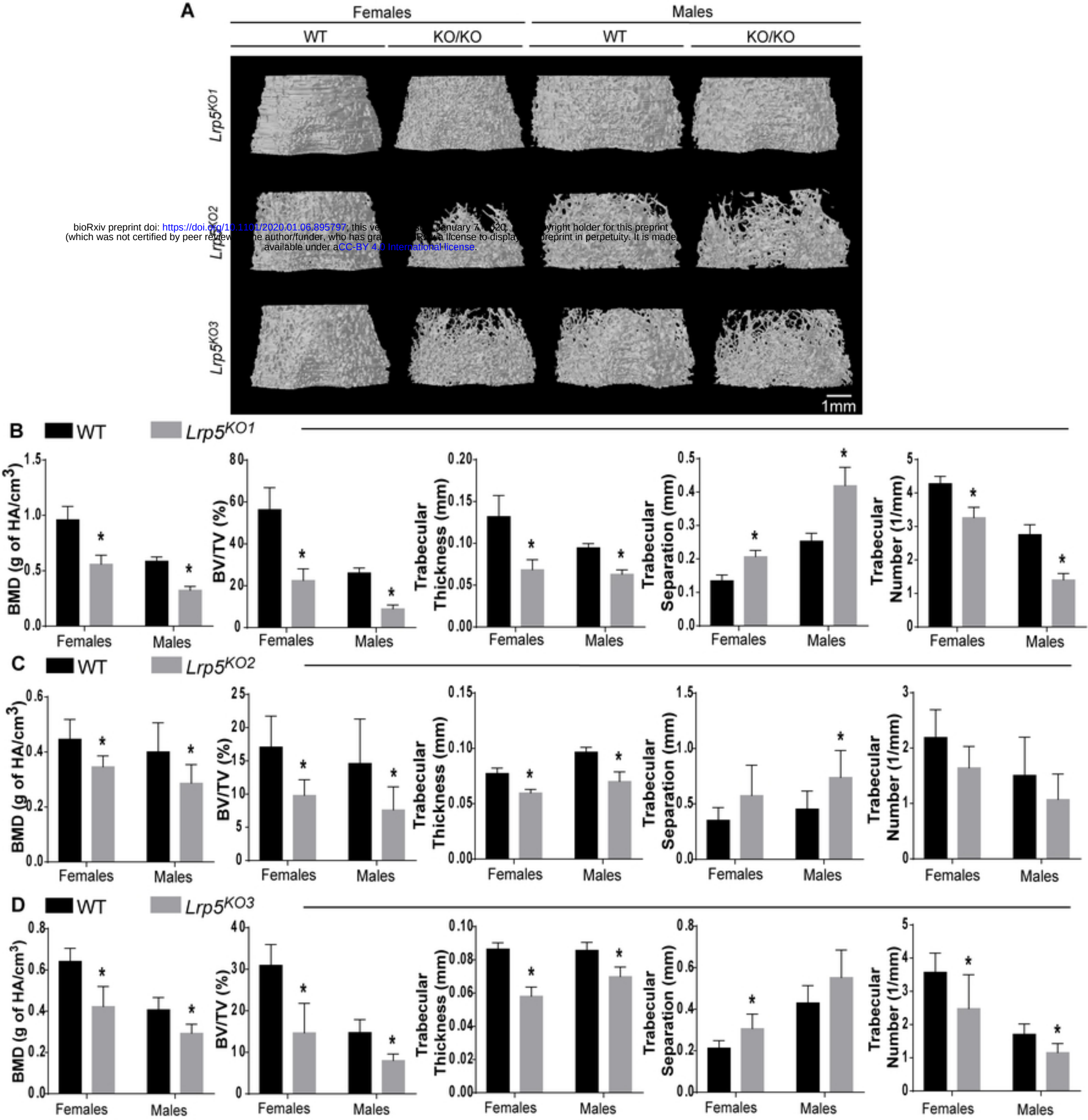

Figure 3

Figure 4

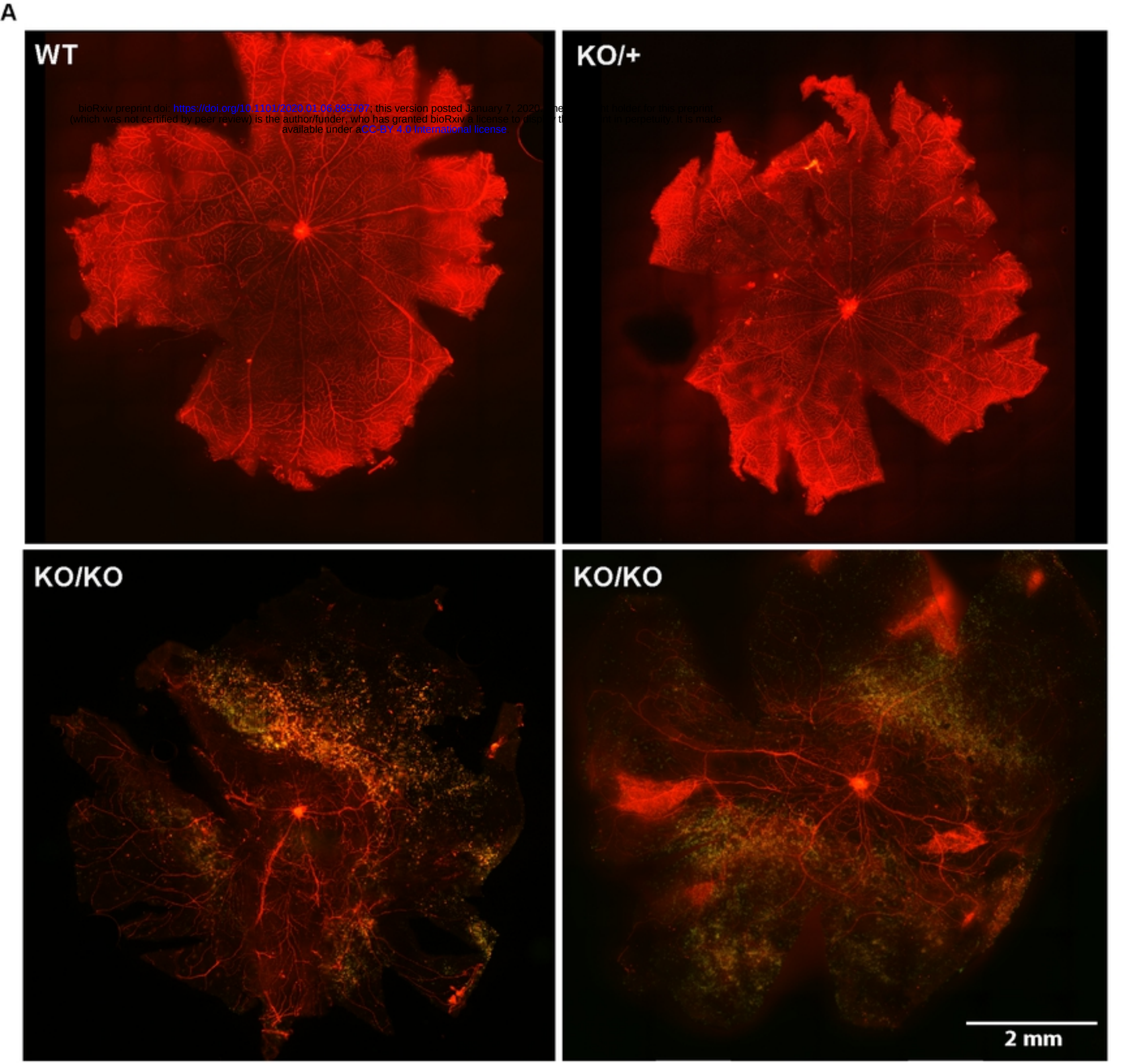

Figure 5

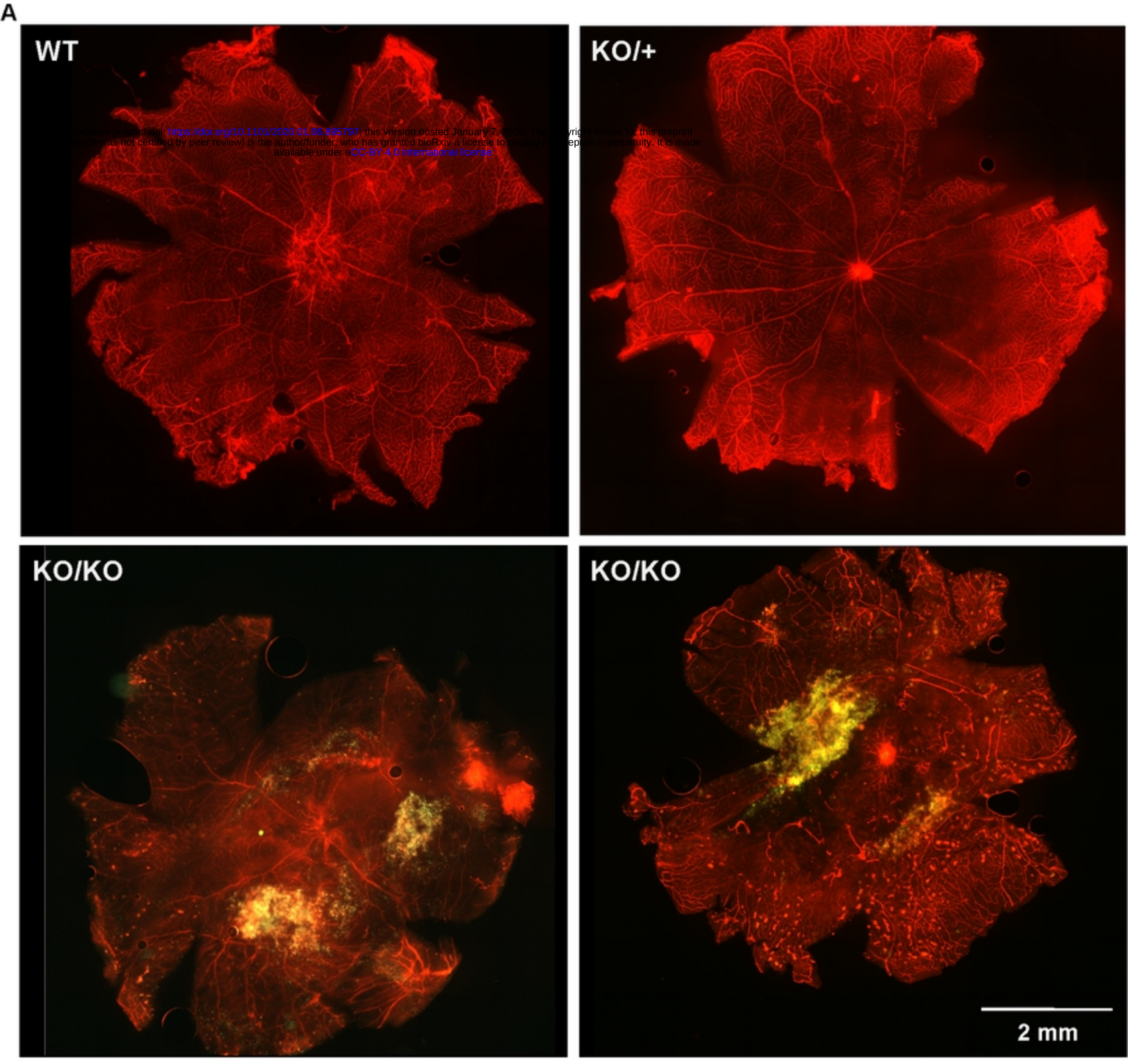

Figure 6

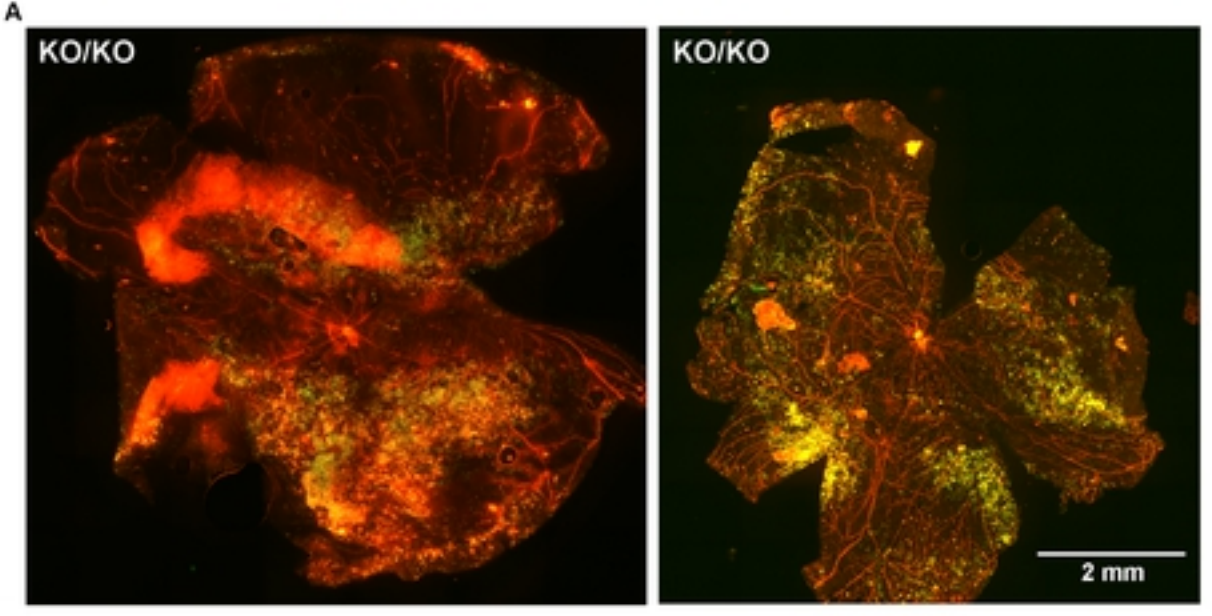

Figure 7

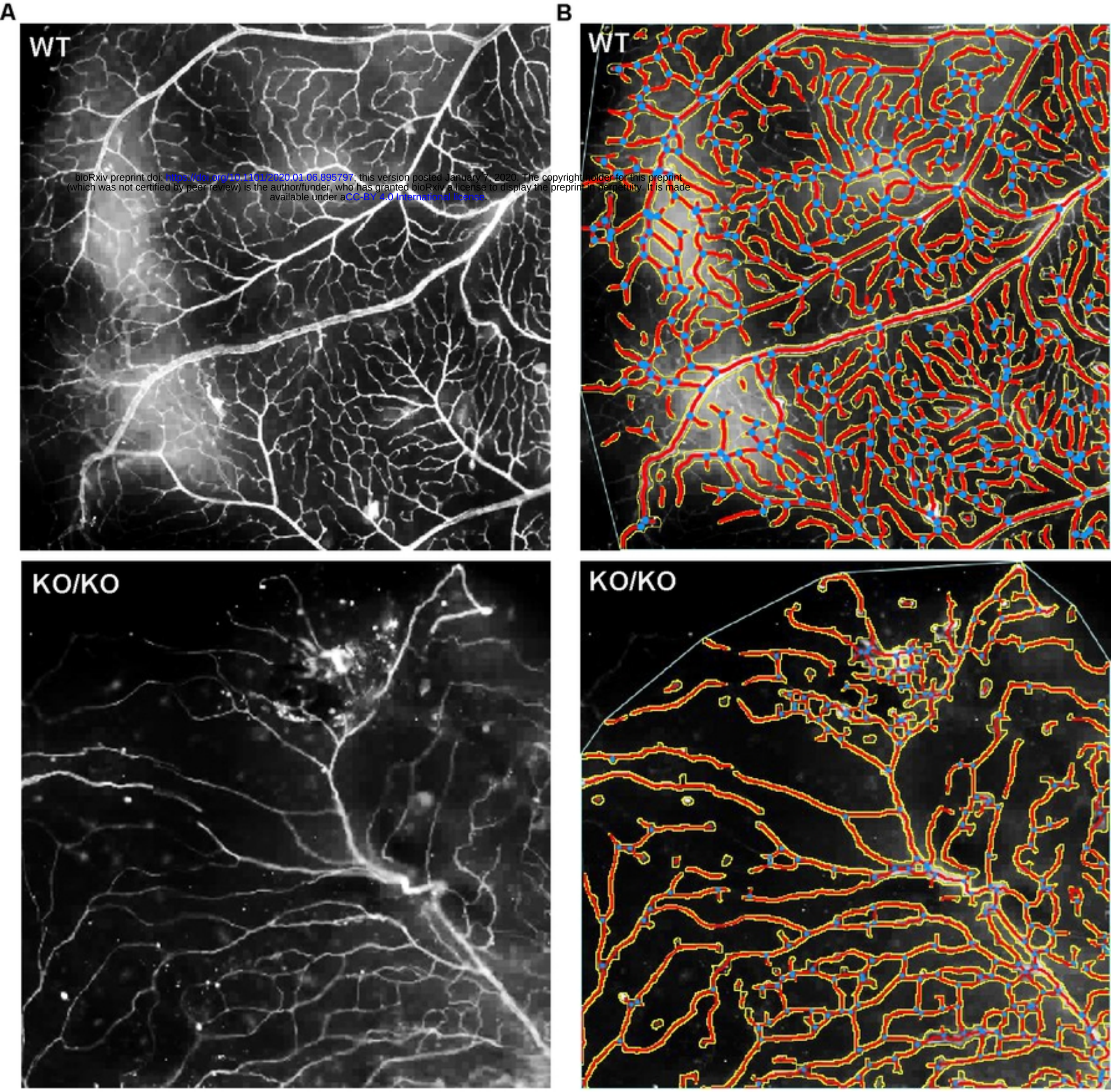

Figure 8

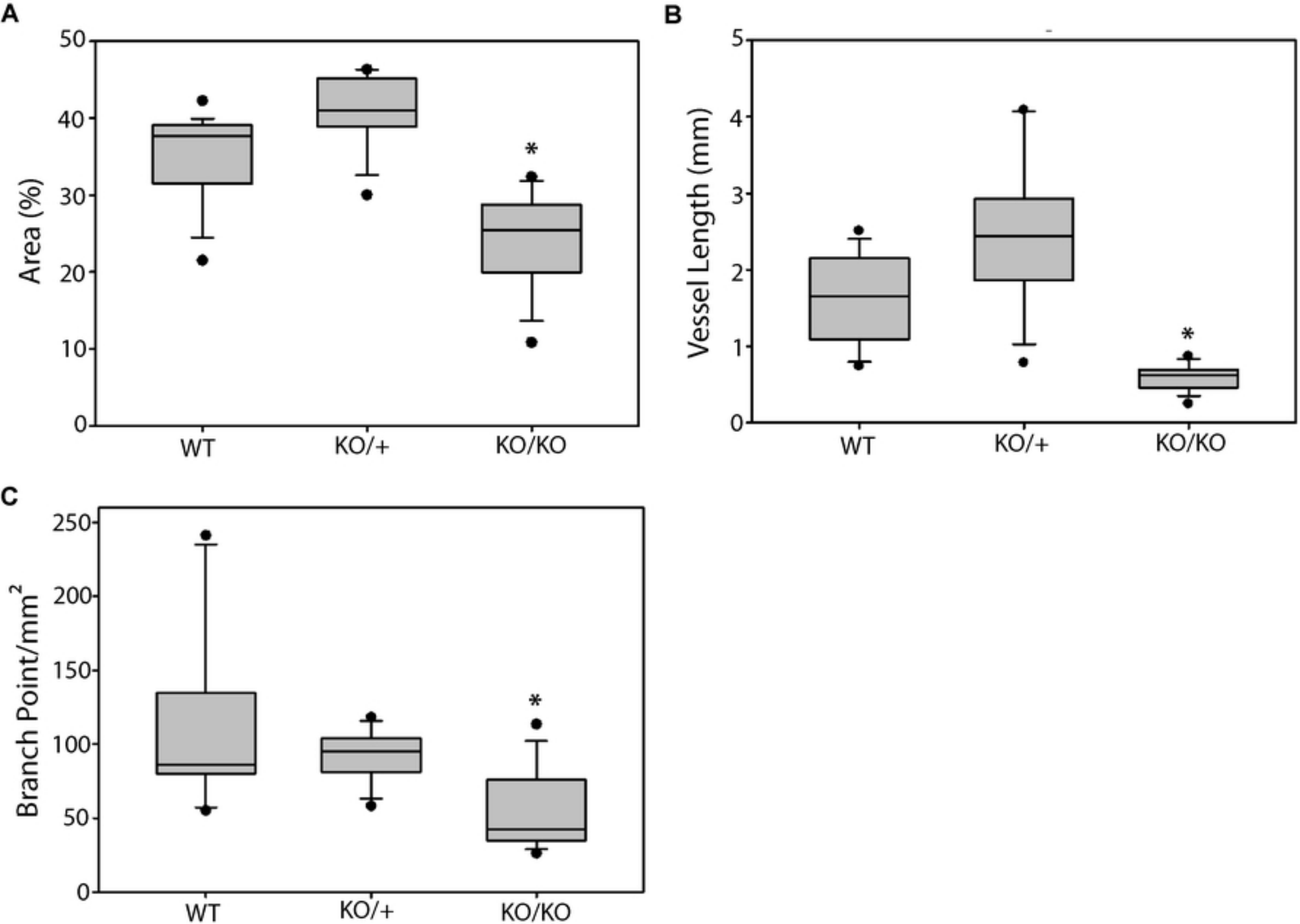
A
Area (%)
50
40
30
20
10
0
WT
KO/+
KO/KO
*
B
Vessel Length (mm)
5
4
3
2
1
0
WT
KO/+
KO/KO
*
C
Branch Point/mm²
250
200
150
100
50
0
WT
KO/+
KO/KO
*

Figure 9

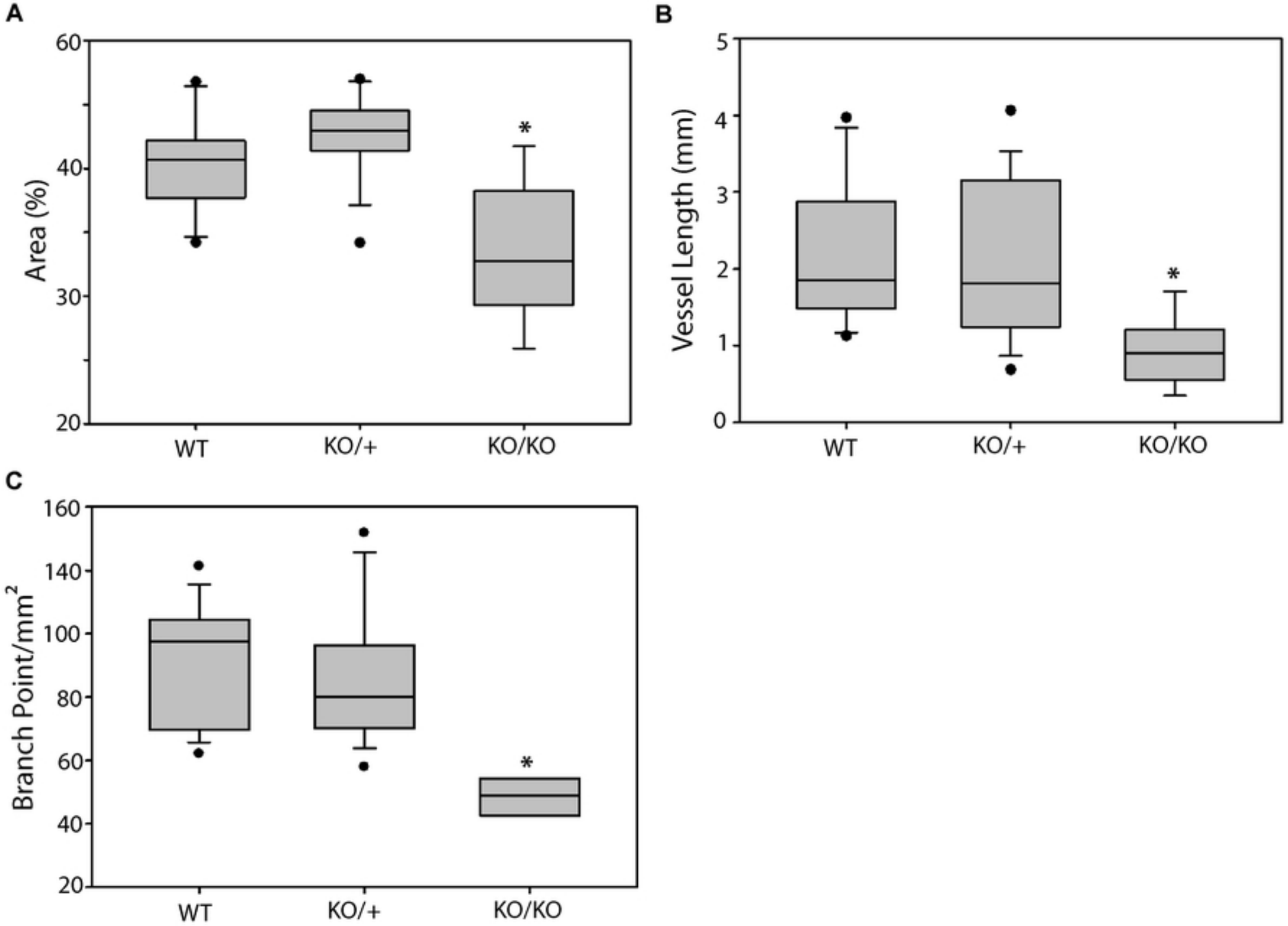
A
60
40
30
20
Area (%)
*
WT
KO/+
KO/KO
B
5
4
3
2
1
0
Vessel Length (mm)
*
WT
KO/+
KO/KO
C
160
140
100
80
60
40
20
Branch Point/mm²
*
WT
KO/+
KO/KO

Figure 10